Talanta 287 (2025) 127576

Contents lists available at ScienceDirect

Talanta

journal homepage: www.elsevier.com/locate/talanta

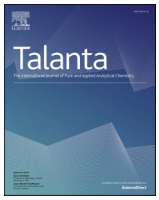

Ratiometric bioluminescent detection of Cu(II) ion based on differences in enzymatic reaction kinetics of two luciferase variants

Ti Wu [a,b], Md Nadim Hossain [b], Mitsuru Hattori [b], Takeharu Nagai [a,b,c,d,*]

[a] Graduate School of Pharmaceutical Science, Osaka University, Suita, Osaka, 565-0871, Japan
[b] SANKEN (The Institute of Scientific and Industrial Research), Osaka University, Ibaraki, Osaka, 567-0047, Japan
[c] Transdimensional Life Imaging Division, Institute for Open and Transdisciplinary Research Initiative, Osaka University, Suita, Osaka, 565-0871, Japan
[d] Research Institute for Electronic Science, Hokkaido University, Sapporo, Hokkaido, 001-0020, Japan

ARTICLE INFO

Keywords:
Cu^{2+}
Bioluminescence
Water
Detection
BRET
NanoLuc
Smartphone

ABSTRACT

Heavy metal contamination in water bodies has raised global concerns due to its significant threats to both public health and ecosystem. Copper (Cu), one of the most widely used metals, is also an essential trace element in physiological systems. Excessive intake of Cu from water can cause toxicity, potentially resulting in serious health risks. Ensuring water safety necessitates the critical detection of copper ion (Cu^{2+}). Here, we report a ratiometric bioluminescent detection method for Cu^{2+}, DERK-Cu(II), which is based on the Distinct Enzymatic Reaction Kinetics of two luciferase variants. In DERK-Cu(II), the blue luminescent luciferase exhibits lower catalytic efficiency than the green luminescent luciferase, thus it is less inhibited by Cu^{2+}. Consequently, the luminescence color of their mixture is dependent on the Cu^{2+} concentrations, enabling us to find an optimal mixing ratio at which luminescence color changes evidently from green to blue. Building on this, we established a quantitative detection method for Cu^{2+} using a smartphone and successfully measured the Cu^{2+} concentrations in several water samples. The method we developed, using the difference in reaction kinetics of two enzymes with the same substrate specificity, would become a versatile approach applicable to the development of other enzyme-based indicators.

1. Introduction

Copper (Cu) is an indispensable trace element for humans. It serves as a key catalytic cofactor in a wide range of physiological processes, including cellular respiration, neurotransmitter metabolism, and redox homeostasis [1–4]. However, an excessive level of Cu in the human body can lead to heavy metal poisoning, causing significant production of reactive oxygen species (ROS) and resulting in oxidative damage to organs [5,6]. A classic disease such as Wilson's disease is also associated with Cu overload [7]. Water is potentially a major resource of Cu exposure for public health [8], as the cupric ion (Cu^{2+}) is the most common oxidation state of Cu in water, with high biological availability [9,10]. Corrosion of the Cu pipes, widely used in household plumbing, is the most common reason for elevated Cu^{2+} level in domestic water [11]. Additionally, with the rising global production of Cu, the continuous release of Cu^{2+} into environmental waters and the consequent threats to ecosystems have become global concerns [12]. Therefore, numerous countries and organizations have established safety guidelines for Cu^{2+} in drinking water, such as < 2 mg/L as recommended by the World Health Organization (WHO) and <1.3 mg/L by the United States Environmental Protection Agency (USEPA) [13].

Detecting Cu^{2+} is an essential task for ensuring safe water use. Representative conventional methods for Cu^{2+} detection include electrochemical analysis, atomic absorption spectroscopy (AAS), inductively coupled plasma optical emission spectrometry (ICP-OES), and inductively coupled plasma mass spectrometry (ICP-MS) [14–18]. Although these methods offer high sensitivity and accuracy, they are costly and time-consuming, requiring professional instruments and well-trained operators. Optical detection of Cu^{2+}, including colorimetric and fluorescent methods based on chemical dyes, nanoparticles, and porous materials, has been extensively developed to simplify procedures [19–21]. However, these methods still require large optical detecting instruments, which hampers their application in portable field analysis. Sun et al. designed an integrated portable device for fluorescence-based Cu^{2+} detection, using a black box equipped with an LED flashlight, smartphone, and so on [22]. However, the components are complex and

* Corresponding author. SANKEN (The Institute of Scientific and Industrial Research), Osaka University, Ibaraki, Osaka, 567-0047, Japan.
E-mail address: ng1@sanken.osaka-u.ac.jp (T. Nagai).

https://doi.org/10.1016/j.talanta.2025.127576
Received 21 September 2024; Received in revised form 8 January 2025; Accepted 10 January 2025
Available online 15 January 2025

unstable; the drift in LED excitation light intensity can affect the reliability. Consequently, the optical detection of Cu^{2+} for field analysis remains limited by various detection conditions.

Bioluminescence, a useful optical tool, is generated through the oxidation of luciferin substrate catalyzed by luciferase [23]. Since this reaction does not require external excitation light, it is particularly well-suited for field analysis [24,25]. All reported bioluminescent Cu^{2+} indicators are of the intensiometric type, relying on Cu^{2+}-responsive caged imidazopyrazinone luciferins to generate "turn-on" intensity signals [26,27]. On the other hand, the ratiometric type of indicator can provide an intuitive signal response through changes in the emission spectrum, enabling a digital or a smartphone camera to capture the bioluminescent image [28–30]. This detection method can significantly reduce the need for professional instruments and operational complexity. To achieve sufficient brightness, many studies have utilized NanoLuc (Nluc) luciferase [31], which was engineered from the marine luciferase, *Oplophorus* luciferase (Oluc) (reference: Osamu Shimomura paper). Nluc is one of the brightest bioluminescent proteins currently known; its conjugation with multiple fluorescent proteins can expand the bioluminescence color palette, based on the principle of bioluminescence resonance energy transfer (BRET) [32]. Nluc has become a comprehensive platform for developing various bioluminescent probes for both *in-vitro* and *in-vivo* detection [33–35].

Interestingly, reports have indicated that the bioluminescence of several marine luciferases, all reacting with the same natural luciferin, coelenterazine, can be potently inhibited by micromolar concentrations of Cu^{2+} [36–39]. The mechanism was identified as a specific reaction between the imidazopyrazinone structure in coelenterazine and Cu^{2+}, leading to the formation of an inert substrate [40]. This characteristic enables the detection of Cu^{2+} through the inhibition of bioluminescence resulting from substrate depletion.

Herein, we developed the first reported bioluminescent ratiometric Cu^{2+} indicator for the *in-vitro* detection of Cu^{2+} that offers high sensitivity and ion selectivity. The sensing principle is based on specific inhibitory effect of Cu^{2+} on the bioluminescence of imidazopyrazinone-based luciferases. We constructed two bioluminescent proteins with different colors based on Nluc, each displaying different Cu^{2+} response levels. The protein mixture, comprising these two proteins mixed at an optimal ratio, exhibited sufficient brightness and a significant emission color change at micromolar concentrations of Cu^{2+}. Using this indicator, we established an easy, rapid, and convenient method for detection of Cu^{2+}, demonstrating its application in copper contaminated and environmental waters using a smartphone camera.

2. Materials and methods

2.1. Gene construction

For the expression of Nluc mutants in *Escherichia coli* (*E. coli*), cDNAs of Nluc were separately amplified into two segments by PCR using KOD-Plus (Toyobo Life Science) and specific primer pairs. These primers contained mutation sequences and the recognition sites of restriction enzymes, *Bam*HI and *Eco*RI, respectively. The oligonucleotide primers were synthesized by Hokkaido System Science. The purified segments served as templates for the subsequent overlapping PCR, facilitating the fusion. For the construction of fNanoBiT, cDNAs of LgBiT and SmBiT (Promega) were fused using overlapping PCR. For the construction of Green-Nluc(D9R), cDNAs of the C-terminal 10 amino acid truncated mNeonGreen and N-terminal 5 amino acid truncated Nluc(D9R) were fused via a linker encoded by "GGGTTT" using overlapping PCR. All cDNA products were then digested with restriction enzymes (Takara-Bio) and extracted from the agarose gel with QIAEX II kit (QIAGEN). The segments were cloned in-frame between *Bam*HI and *Eco*RI sites in pRSETB vector (Invitrogen) using T4 ligase in Rapid Ligation Buffer (Promega). The transformation of *E. coli* strain XL-10 gold with the ligated plasmids was carried out using heat shock. Plasmid DNAs were purified from cultured *E. coli* using the alkali-SDS method. The sequences were verified using dye terminator cycle sequencing with the BigDye Terminator v1.1 Cycle Sequencing kit (Thermo Fisher Scientific).

2.2. Protein purification

Bioluminescent proteins were produced in *E. coli* strain JM109(DE3), which was cultured in 200 mL of LB bacterial medium containing 0.1 mg/mL carbenicillin at 23 °C for 60 h. Harvested cells were gently diluted in 10 mL of PBS and lysed using a French Press (Thermo Fisher Scientific). Proteins were purified through affinity chromatography on a Ni-NTA column (QIAGEN). The buffer was exchanged to 20 mM HEPES (pH 7.2) using a PD-10 desalting column (GE Healthcare). Protein concentrations were determined using the Bradford method (Protein assay kit, BioRad). The purified proteins were rapidly frozen in liquid nitrogen and stored at −80 °C.

2.3. Ion selectivity test

Aqueous solutions of metal ions were prepared by dissolving LiCl, NaCl, KCl, $MgCl_2$, $CaCl_2$, RbCl, $MnCl_2$, $FeCl_3$, $CoCl_2$, $NiCl_2$, $ZnCl_2$, $CuCl_2$, $CdCl_2$, and $PbCl_2$ (Wako Chemicals) in Milli-Q water. 100 μL of 2 nM purified protein (20 mM HEPES, pH 7.2) was loaded into a 96-well plate, followed by the addition of each metal ion to a final concentration of 2 μM. The bioluminescence intensity of each well was measured 20 s after the addition of coelenterazine-h (CTZ-h) (Wako Chemicals) using a microplate reader (SH-9000, Corona Electric).

2.4. Measurement of bioluminescence intensity upon addition of Cu^{2+}

A series of Cu^{2+} solutions with concentrations ranging from 0 to 10 μM was prepared in advance. 100 μL of 2 nM purified Nluc and its variants (20 mM HEPES, pH 7.2) were mixed with 50 μL of Cu^{2+} solutions, achieving final concentration ranging from 0 to 2 μM. Bioluminescence intensities were measured using a microplate reader 20 s after adding 100 μL of 5 μM CTZ-h. The normalized intensities were plotted against Cu^{2+} concentrations, with fitting curves obtained from dose-response nonlinear regression analysis (GraphPad Prism 9.5).

2.5. Titration of CTZ-h on luciferase activity

CTZ-h was initially dissolved in methanol to a concentration of 5 mM and then refrigerated. Before titration, CTZ-h was diluted to 0.05, 0.1, 0.2, 0.4, 0.8, 1.6, 3.3, and 6.5 μM using HEPES (20 mM, pH 7.2). 50 μL of 2 nM purified proteins were loaded into a 96-well plate, followed by the addition of 50 μL of CTZ-h at various concentrations using an automatic dispenser in a microplate reader. The initial bioluminescence was measured within 12 s after adding CTZ-h. To convert relative luminescence units into photon numbers, a luminol chemiluminescence standard was used for calibration [41]. The calculated initial velocities (photons/s) were plotted against the concentration of CTZ-h and fitted to the Michaelis-Menten equation (GraphPad Prism 9.5).

2.6. Ratiometric detection of Cu^{2+} using developed method

For detection using a smartphone camera, 100 μL of 50 nM mixed proteins and 50 μL of Cu^{2+} solutions were added to a 96-well plate. 100 μL of 5 μM CTZ-h was manually dispensed into each well using a multichannel pipette. The image was captured using a smartphone camera (HUAWEI P40 Pro) 30 s after the substrate was added. The camera was positioned perpendicular to the plate and the image was captured in the dark, under the following settings: ISO 6400, exposure time of 1/10 s, white balance of 6000, and manual focus. The image was transferred to a computer and separated into three color channels (blue, green, and red) using ImageJ software. The intensity of each channel was calculated as

the average value within each well. The calculated color ratios were plotted against Cu^{2+} concentrations and modeled using an exponential growth curve. The limit of detection (LOD) was calculated using the formula $R_{LOD} = R_0 + 3\sigma_0$, where R_{LOD} represents the ratio of detection limit, R_0 is the average of blank ratios, and σ_0 is the standard deviation of the blank ratios. For spectral measurements, the reaction mixture was individually loaded into a transparent cuvette. The spectrum was measured 30 s after the substrate was added, using a multi-channel spectrophotometer (PMA-12, Hamamatsu Photonics) with an exposure time of 5 s.

2.7. Preparations of water samples

For copper contaminated water samples, various amounts of copper solids were immersed in 10 ml of 0.1 M NaCl solution overnight. Standard solutions were prepared by dissolving $CuCl_2$ powder in the same NaCl solution. For environmental water samples, sample 1 and 2 were collected from the rivers in Ginzan, Inagawcho, Hyogo prefecture, Japan. Sample 3 was collected from the moat surrounding Nisanzai Kofun, Mozu Nishinocho, Sakai, Osaka, Japan. All collected samples were filtered with a 0.22 μM membrane filter (MilleX-GP, Merck Millipore Ltd) and acidified with 3 M nitric acid for preservation. Prior to testing, the pH was adjusted to 7.2 with 10 mM HEPES. The standard solutions were prepared using $CuCl_2$ powder dissolved in the same buffer.

2.8. Detection of Cu^{2+} in water samples

For detecting copper contaminated water, 50 μL of standard Cu^{2+} solutions ranging from 0 to 10 μM and three samples were loaded into each well of a 96-well plate, along with 100 μL of 50 nM protein indicator. 100 μL of 5 μM CTZ-h was simultaneously added using a multichannel pipette, and an image was captured with a smartphone camera 30 s later. The smartphone camera setting was as follows: ISO 6400, exposure time of 1/10 s, white balance of 6000, and manual focus. For environmental water detection, 100 μL of standard Cu^{2+} solutions ranging from 0 to 2 μM and three samples were loaded into each well, along with 100 μL of 50 nM protein indicator. All the other conditions were identical to those used for the copper contaminated water samples. To determine the Cu^{2+} concentration (C), the regression relationship $R = R_0 * \exp(k * C)$ was established based on data from each set of standard wells. Here, R represents the ratio of the blue to green channel intensities, and R_0 and k are parameters derived from the non-linear fitting. The Cu^{2+} concentration in the sample was determined by calculating $C = \ln(R/R_0)/k$. As a control method, ICP-OES (ICPS-8000, SHIMADZU) was employed to measure the samples, following the operational manual.

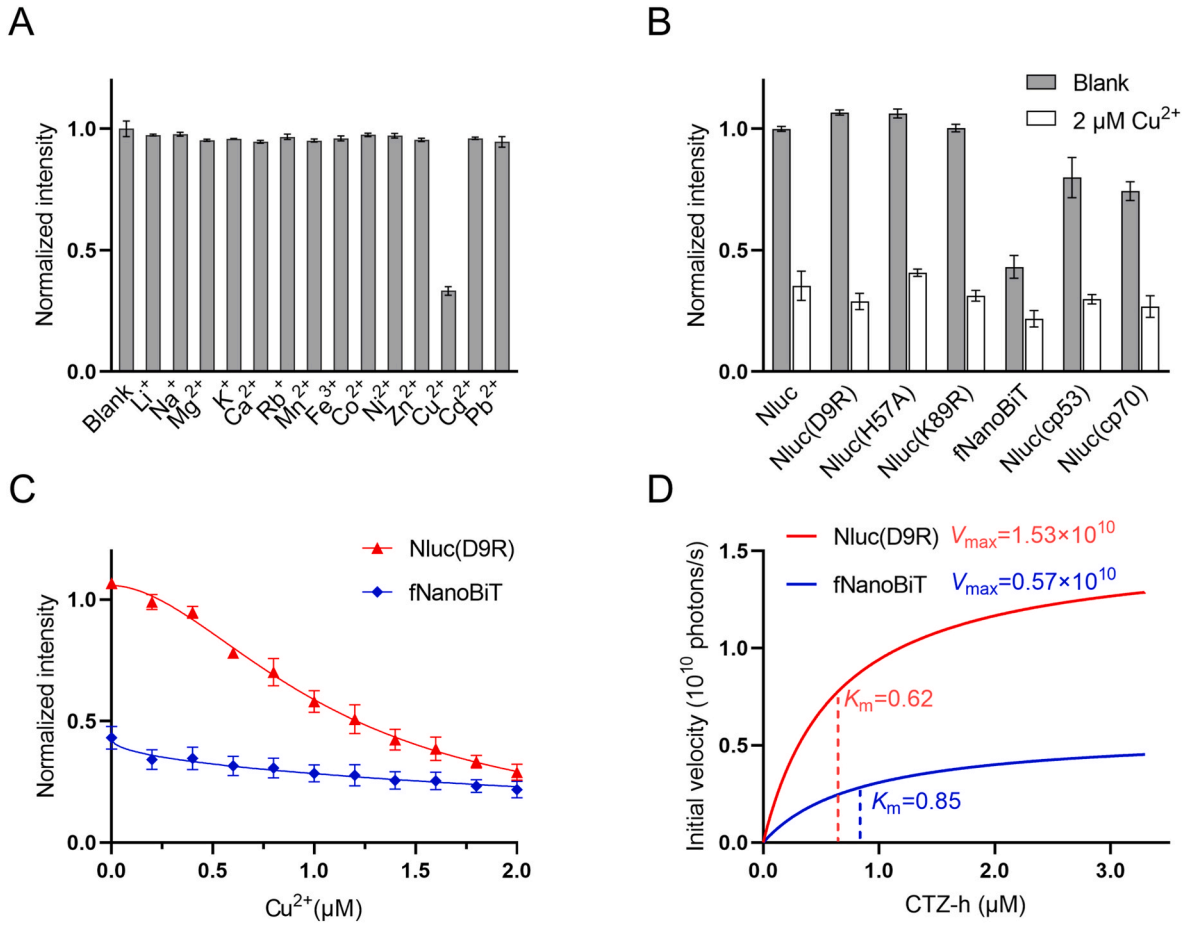

Fig. 1. Inhibition of bioluminescence by Cu^{2+} in Nluc and its related variants. (A) Metal ion selectivity in inhibition of Nluc bioluminescence. The bioluminescence of Nluc was measured in the presence of various metal ions. The data were normalized against the intensity of the blank control. (B) Comparison of bioluminescence intensity of Nluc and its related variants in the presence of Cu^{2+}. The intensities were normalized to the Nluc intensity of the blank. (C) Cu^{2+} dose-response curves of Nluc(D9R) and fNanoBiT variants. The data were fitted to an inhibitor dose-response equation. (D) Titration curves of CTZ-h illustrating the initial reaction velocity of Nluc(D9R) and fNanoBiT. The data were fitted to the Michaelis-Menten equation. Average data and standard deviations across all figures are presented for $n = 3$.

3. Results and discussion

3.1. Difference in inhibitory effect of Cu^{2+} on bioluminescence among luciferase variants

First, we analyzed the inhibitory effect of Cu^{2+} on the reaction between Nluc and CTZ-h, an analogue of native coelenterazine with enhanced intensity [42]. The ion selectivity test, using Nluc with CTZ-h as a substrate, demonstrated that Cu^{2+} specifically inhibited the bioluminescence intensity of Nluc compared to other common metal ions (Fig. 1A). This result suggested that Nluc and CTZ-h could be effectively used for the specific detection of Cu^{2+}. Based on the knowledge that Cu^{2+} inhibition of bioluminescence is due to luciferin inactivation, we hypothesized that the extent of Cu^{2+} inhibition might vary depending on the different catalytic efficiencies of luciferase for the luciferin substrate. To test this hypothesis, we prepared a series of Nluc variants including the variants with single amino acid mutant (D9R, H57A, and K89R), the circularly permuted variants (cp53 and cp70), and the fusion type of NanoBiT (fNanoBiT), which was created by fusing two subunits of a split Nluc system (Fig. S9) [43,44]. We compared the changes in bioluminescence intensities of these variants in the presence or absence of Cu^{2+} (Fig. 1B). Cu^{2+} inhibited the bioluminescence of each variant differently. Among these, the greatest differences in inhibition rates were observed in the D9R variant (73 %) and the fNanoBiT variant (49 %). In the Cu^{2+} dose-response curves for these two variants, the decrease in bioluminescence of fNanoBiT occurred relatively gradually (Fig. 1C). The inhibition slopes of the Cu^{2+} dose-response curves were −1.84 for Nluc(D9R) and −0.46 for fNanoBiT, indicating that Cu^{2+} significantly affects the bioluminescence reaction of Nluc(D9R) to a greater extent than that of fNanoBiT. To clarify this difference in bioluminescence inhibition among luciferases from a reaction kinetics perspective, luciferin titrations were performed to calculate the initial reaction velocities. Nluc(D9R) exhibited higher catalytic efficiency than fNanoBiT, as demonstrated by its higher Vmax and lower Km (Fig. 1D). During substrate depletion, enzymes with high catalytic efficiency exhibited a significant decrease in reaction velocity as substrate concentration diminished. Therefore, Nluc(D9R) was found to be more inhibited by Cu^{2+} than fNanoBiT, attributed to its higher catalytic efficiency toward the substrate.

3.2. Development of bioluminescent proteins with different colors and Cu^{2+} dose-responses

Leveraging the difference in reaction kinetics between Nluc(D9R) and fNanoBiT, a new detection method for Cu^{2+} can be developed. When the bioluminescence of both is detected simultaneously, it becomes necessary to distinguish between them by modifying the wavelength. We conceived the idea of altering the emission color of luciferase through the use of BRET. The green fluorescent protein "mNeonGreen" was selected as the energy acceptor because of its high brightness [45]. It was confirmed that mNeonGreen itself exhibits no significant fluorescence fluctuation in the presence of common metal ions (Fig. S4). We then constructed a fusion protein of Nluc(D9R) and mNeonGreen (Green-Nluc(D9R)) (Fig. 2A). The emission color shifted greatly from blue peaking at 460 nm to green peaking at 520 nm (Fig. 2B). To determine the Cu^{2+}-dependent intensity changes of these two emission colors, the bioluminescence was quantitatively measured using a microplate reader. The result showed that the bioluminescence intensity ratio of the two proteins gradually increased as the Cu^{2+} concentration ranged from 0 to 2 μM. This suggests that the ratio of bioluminescence from these two different colors could be utilized to detect Cu^{2+} concentrations (Fig. 2C).

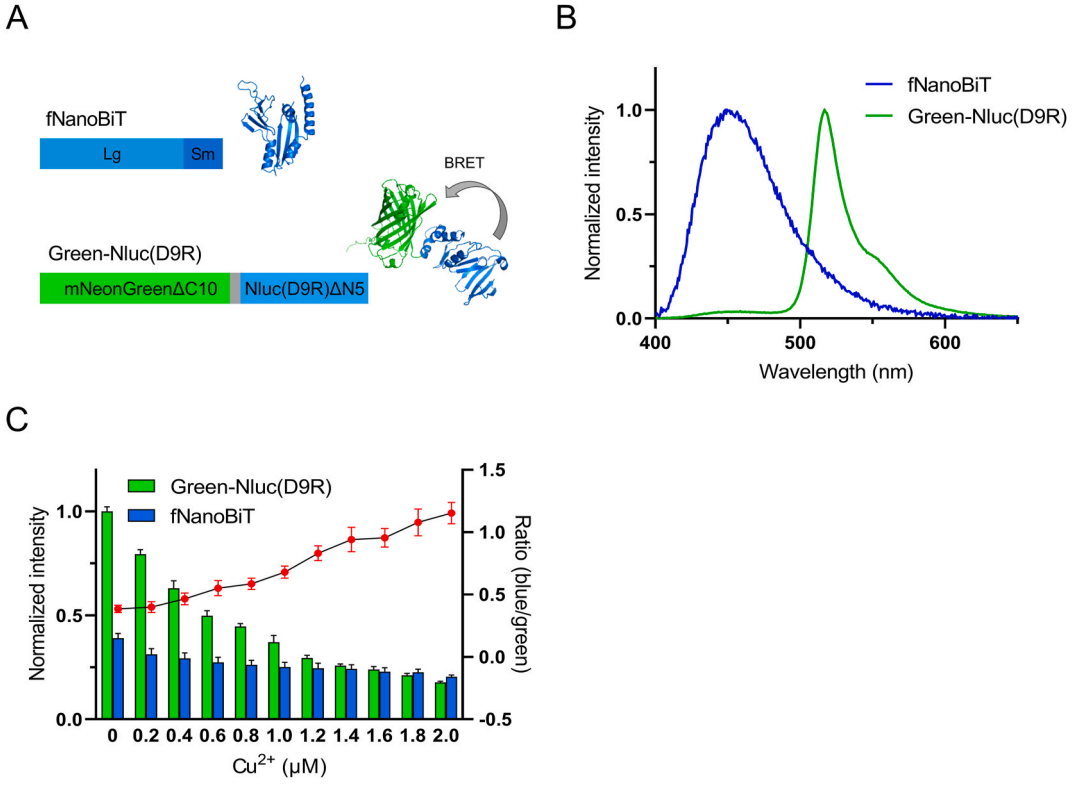

Fig. 2. Development of two bioluminescent proteins with distinct colors and varying levels of Cu^{2+} inhibition. (A) Schematic illustration of fNanoBiT and Green-Nluc (D9R): fNanoBiT is a fusion of LargeBiT (Lg) and SmallBiT (Sm); Green-Nluc(D9R) is a fusion of mNeonGreen and Nluc(D9R) connected with the linker, GGGTTT (gray). (B) Bioluminescence spectra of fNanoBiT and Green-Nluc(D9R), normalized to their respective peak values. (C) Cu^{2+} dose-responses for fNanoBiT and Green-Nluc(D9R), measured with a microplate reader. Intensity ratios were calculated and plotted; average values and standard deviations are presented for $n = 3$. (For interpretation of the references to color in this figure legend, the reader is referred to the Web version of this article.)

3.3. Ratiometric detection of Cu^{2+} using a smartphone camera

The bioluminescence emitted from Nluc is sufficiently bright for detection with non-professional optical detectors such as smartphone cameras, offering convenience and portability [28,30]. Consequently, we detected the bioluminescence of the two proteins with the addition of Cu^{2+}, using a smartphone (Fig. S5). Since the different intensity changes of these two proteins in response to Cu^{2+} were evident in the image, it was hypothesized that the emission color of their mixture could be altered by Cu^{2+}. To analyze the color change, the original smartphone image was split into blue, green, and red color channels. By mixing these two proteins at different ratios, we compared their color ratios (blue/-green) in scenarios with or without Cu^{2+} (Fig. S6). When fNanoBiT and Green-Nluc(D9R) were mixed at a 2:1 ratio, the bioluminescence color ratio exhibited a change of nearly 160 %, caused by 2 μM of Cu^{2+}. The dominant color of the mixed bioluminescence, initially green, shifted to blue in the presence of Cu^{2+}. This color shift was also clearly documented through emission spectral measurements using a spectrophotometer (Fig. 3A). We explored a procedure for effectively detecting this Cu^{2+}-dependent color changing process using a smartphone camera (Fig. 3B). Given that time-dependent bioluminescence decay may influence the overall color appearance, it is crucial to detect the reaction mixtures at the same time point after the reaction initiates. The substrate was simultaneously added to all samples using a multi-channel pipette. Under optimized conditions, the bioluminescent image captured by the smartphone camera revealed a Cu^{2+}-dependent gradient color transition from green to blue (Fig. 3C). The ratios of blue to green color were plotted against Cu^{2+} concentrations on the graph (Fig. 3D). The exponential growth curve displayed a nearly linear increase in the color ratio as Cu^{2+} concentration ranged from 0 to 2 μM, demonstrating a high correlation efficiency ($R^2 = 0.98$). The limit of detection (LOD) was calculated to be 0.16 μM through the calculation. We named this Cu^{2+} detection method, which utilizes Distinct Enzymatic Reaction Kinetics, as "DERK-Cu(II)". To confirm the smartphone camera detection results by an alternative method, the same measurements were performed using a spectrophotometer (Fig. S7). The results from both methods were highly consistent, confirming the reliability of using a smartphone camera as a detector for detecting the changes in emission color ratios (Fig. S8). To assess the impact of pH on our detection method, we analyzed the emissions of the indicator both with and without Cu^{2+} at various pH levels, employing a range of HEPES buffers. The findings revealed that pH variation significantly affected the emission color ratios. (Fig. S9). Therefore, we underscored the importance of employing a buffer solution to ensure consistent pH in reaction mixtures, thereby minimizing potential errors due to pH fluctuations.

3.4. Competitive ion selectivity

To verify the selectivity and reliability of DERK-Cu(II), we assessed its performance in the presence of various common metal ions. Li^+, Na^+, K^+, Mg^{2+}, Ca^{2+}, Rb^+, Mn^{2+}, Fe^{3+}, Co^{2+}, Ni^{2+}, Zn^{2+}, Cd^{2+}, and Pb^{2+} were added to the reaction mixture at ten times the equivalent of Cu^{2+} (Fig. 4). The results indicated that these ions did not independently "turn on" the signals nor significantly affect the bioluminescence color ratios when co-added with Cu^{2+}. Therefore, the developed detection method demonstrates high selectivity for Cu^{2+} and maintains a stable response in the presence of other metal ions, enabling its use in analyzing complex samples.

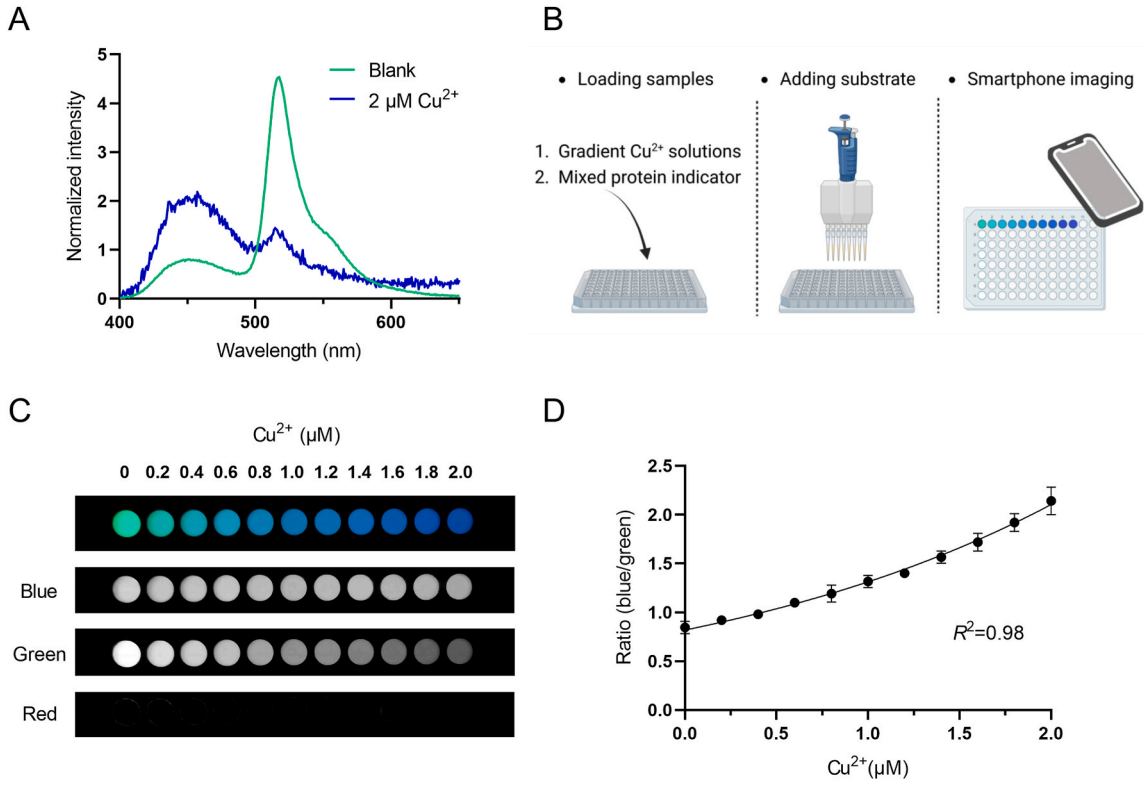

Fig. 3. Ratiometric detection of Cu^{2+} using a combination of two developed bioluminescent proteins. (A) Bioluminescent spectra of mixed proteins, in the presence and absence of 2 μM Cu^{2+}, were normalized to the intensity at 500 nm. (B) Schematic of the procedures used for Cu^{2+} detection with a smartphone camera. (C) Bioluminescent image captured by a smartphone camera of the protein mixtures treated with various concentrations of Cu^{2+}. The original image was divided into three color channels: blue, green, and red. (D) Changes in emission ratios depending on Cu^{2+} concentration. Intensity ratios between the blue and green channels were calculated from the image shown in C. The figure displays a fitting curve derived from the exponential growth equation. Averaged data and standard deviations are presented for $n = 3$. (For interpretation of the references to color in this figure legend, the reader is referred to the Web version of this article.)

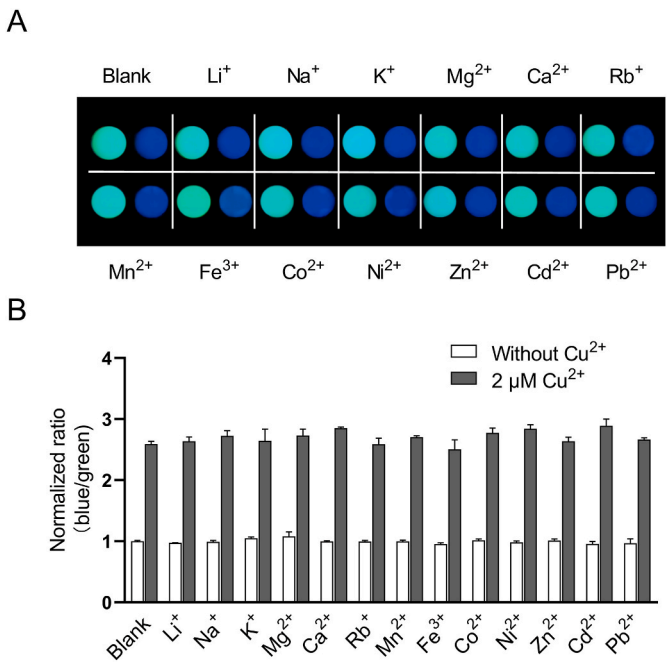

Fig. 4. Competitive ion selectivity of DERK-Cu(II). (A) Bioluminescent images of the reaction mixtures with higher concentrations (20 μM) of different metal ions, captured by a smartphone camera. The right well of each grid was added with 2 μM of Cu^{2+}. (B) Bioluminescent color ratios were measured in the absence (white) and presence (gray) of Cu^{2+}, under varying metal ion conditions. Data were normalized against the blank's ratio without Cu^{2+}. Average values and standard deviations for $n = 3$ are presented. (For interpretation of the references to color in this figure legend, the reader is referred to the Web version of this article.)

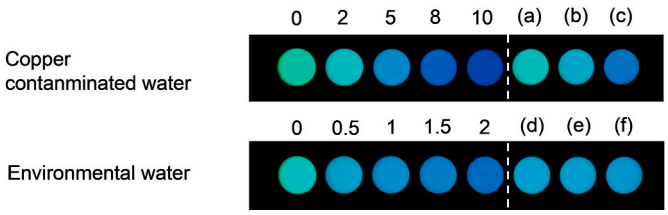

Sample	No.	Developed method (μM)	ICPS-8100 (μM)
Copper contaminated water	(a)	1.37 ± 0.16	1.32 ± 0.02
	(b)	2.87 ± 0.26	3.10 ± 0.03
	(c)	5.83 ± 0.14	6.00 ± 0.13
Environmental water	(d)	0.49 ± 0.02	0.53 ± 0.01
	(e)	0.57 ± 0.07	0.60 ± 0.01
	(f)	0.69 ± 0.06	0.73 ± 0.01

Fig. 5. Detection of Cu^{2+} in water samples using DERK-Cu(II). Bioluminescent images showing the quantitative detection of Cu^{2+} in samples of copper contaminated water (50 μL) and environmental water (100 μL). The images were captured using a smartphone camera. The image indicates the Cu^{2+} concentrations of the standard solutions (in wells to the left of the dashed line) and the sample labels (a–f) (in wells to the right of the dashed line). The table below displays the analyzed results. Average values and standard deviations for $n = 3$ are presented.

3.5. Detection of Cu^{2+} in water samples

Due to its high sensitivity and stable signal response, DERK-Cu(II) can be used for the quantitative detection of Cu^{2+}. To demonstrate its applicability, we used two practical samples. The first sample, copper contaminated water, refers to water with elevated Cu^{2+} levels resulting from the dissolution of solid copper, this simulates the issue of Cu^{2+} contamination in domestic water caused by copper products (Fig. 5 copper contaminated water). The samples were prepared by immersing solid copper in NaCl solution overnight to accelerate the release of soluble Cu^{2+} due to increased corrosion rate [46]. The second sample is river water, demonstrating the applicability for environmental monitoring. Samples were collected from rivers in an old industrial area and from a moat surrounding an ancient tomb (known as KOFUN in Japanese). Insoluble impurities and microorganisms were removed through filtering. Given the low Cu^{2+} concentration in environmental water, the sample volume in the reaction mixture was increased to 100 μL to cover the detection range (Fig. 5 environmental water). Quantitative detection was conducted by referring to the concentrations of corresponding standard solutions and using a smartphone camera (Fig. 5). To verify the accuracy of the developed method, ICP-OES was employed as a control method. The Cu^{2+} concentrations measured by the developed method were in high agreement with those of the control method, with errors less than 8 %. This result confirms that DERK-Cu(II) is highly accurate for the quantitative detection of soluble Cu^{2+} in water.

4. Conclusion

In this study, we demonstrated the development, characterization, and application of the bioluminescent protein-based Cu^{2+} detection method, DERK-Cu(II). To the best of our knowledge, this is the first reported ratiometric type of bioluminescent Cu^{2+} detection. The sensing principle is based on the potent Cu^{2+} inhibitory effect on the bioluminescence of imidazopyrazinone-based luciferase, as reported in several natural luciferases [36–39]. We achieved ratiometric detection by leveraging the difference in Cu^{2+} dose-responses among luciferase variants, attributable to distinct kinetic properties, and by distinguishing their bioluminescent emission spectra using the BRET strategy. The ratiometric detection offers the advantage of providing a more intuitive readout, as it directly reflects Cu^{2+} concentration through the change in bioluminescence color. The developed method exhibits high sensitivity and selectivity at micromolar concentrations of Cu^{2+}. These characteristics enable the quantitative detection of Cu^{2+} in water samples.

Notably, due to its high brightness and significant color changes, DERK-Cu(II) can be performed using a smartphone camera. It does not require any professional detection instruments, significantly enhancing convenience and portability. Using this method, we successfully detected Cu^{2+} in copper contaminated and environmental waters with high accuracy. Collectively, the demonstrated results suggest that DERK-Cu (II) offers an easy, rapid, and convenient detection for the field analysis of Cu^{2+} in water.

Moreover, the DERK approach in this study, which employs a two-luciferase system based on distinct enzymatic reaction kinetics, would contribute to the development of other target detections. For example, applying DERK to luciferase-antigen fusion proteins for antibody detection could lead to new immunoassays, potentially simplifying operation and reducing equipment requirements. We expect DERK to become a versatile approach for developing multiple indicators for rapid field analysis and point-of-care diagnosis.

CRediT authorship contribution statement

Ti Wu: Writing – original draft, Validation, Investigation, Data curation. **Md Nadim Hossain:** Investigation, Data curation. **Mitsuru Hattori:** Writing – review & editing, Validation, Funding acquisition. **Takeharu Nagai:** Writing – review & editing, Supervision, Project administration, Funding acquisition, Conceptualization.

Declaration of competing interest

The authors declare that they have no known competing financial interests or personal relationships that could have appeared to influence the work reported in this paper.

Acknowledgement

This study was partially supported by grants from Ministry of Education, Culture, Sports, Science, and Technology (MEXT) (No. 18H05410 to T.N.), Japan Society for Promotion of Science (JSPS) (No. 22K05143 to M.H.), JST CREST Program (No. JPMJCR20H9 to T.N.), Takeda Science Foundation (to T.N.), Uehara Memorial Foundation (to T.N.), and Kobayashi Foundation Scholarship (to T.W.).

Appendix A. Supplementary data

Supplementary data to this article can be found online at https://doi.org/10.1016/j.talanta.2025.127576.

Data availability

Data will be made available on request.

References

[1] K. Jomova, M. Makova, S.Y. Alomar, S.H. Alwasel, E. Nepovimova, K. Kuca, C. J. Rhodes, M. Valko, Essential metals in health and disease, Chem. Biol. Interact. 367 (2022) 110173, https://doi.org/10.1016/j.cbi.2022.110173.

[2] P. Iñarrea, H. Moini, D. Han, D. Rettori, I. Aguiló, M.A. Alava, M. Iturralde, E. Cadenas, Mitochondrial respiratory chain and thioredoxin reductase regulate intermembrane Cu, Zn-superoxide dismutase activity: implications for mitochondrial energy metabolism and apoptosis, Biochem. J. 405 (1) (2007) 173–179, https://doi.org/10.1042/BJ20061809.

[3] S. Lutsenko, A. Bhattacharjee, A.L. Hubbard, Copper handling machinery of the brain, Metallomics 2 (9) (2010) 596–608, https://doi.org/10.1039/c0mt00006j.

[4] L.M. Gaetke, C.K. Chow, Copper toxicity, oxidative stress, and antioxidant nutrients, Toxicology 189 (1–2) (2003) 147–163, https://doi.org/10.1016/S0300-483X(03)00159-8.

[5] J. Chen, Y. Jiang, H. Shi, Y. Peng, X. Fan, C. Li, The molecular mechanisms of copper metabolism and its roles in human diseases, Pflügers Archiv 472 (2020) 1415–1429, https://doi.org/10.1007/s00424-020-02412-2.

[6] B. Ashish, K. Neeti, K. Himanshu, Copper toxicity: a comprehensive study, Res. J. Recent Sci. 2277 (2013) 2502. https://www.isca.me/rjrs/archive/special_issue2012/12.ISCA-ISC-2012-4CS-93.pdf.

[7] L. Chen, J. Min, F. Wang, Copper homeostasis and cuproptosis in health and disease, Signal Transduct. Targeted Ther. 7 (1) (2022) 378, https://doi.org/10.1038/s41392-022-01229-y.

[8] D.J. Fitzgerald, Safety guidelines for copper in water, Am. J. Clin. Nutr. 67 (5) (1998) 1098S–1102S, https://doi.org/10.1093/ajcn/67.5.1098S.

[9] C.A. Flemming, J.T. Trevors, Copper toxicity and chemistry in the environment: a review. Water, Air. Soil. Pollut. 44 (1989) 143–158, https://doi.org/10.1007/BF00228784.

[10] L.M. Gaetke, H.S. Chow-Johnson, C.K. Chow, Copper: toxicological relevance and mechanisms, Arch. Toxicol. 88 (2014) 1929–1938, https://doi.org/10.1007/s00204-014-1355-y.

[11] M. Rehman, L. Liu, Q. Wang, M.H. Saleem, S. Bashir, S. Ullah, D. Peng, Copper environmental toxicology, recent advances, and future outlook: a review, Environ. Sci. Pollut. Res. 26 (2019) 18003–18016, https://doi.org/10.1007/s11356-019-05073-6.

[12] G. Izydorczyk, K. Mikula, D. Skrzypczak, K. Moustakas, A. Witek-Krowiak, K. Chojnacka, Potential environmental pollution from copper metallurgy and methods of management, Environ. Res. 197 (2021) 111050, https://doi.org/10.1016/j.envres.2021.111050.

[13] R. Manne, M.M.R.M. Kumaradoss, R.S.R. Iska, A. Devarajan, N. Mekala, Water quality and risk assessment of copper content in drinking water stored in copper container, Appl. Water Sci. 12 (3) (2022) 27, https://doi.org/10.1007/s13201-021-01542-x.

[14] A.M. Elkhatat, M. Soliman, R. Ismail, S. Ahmed, N. Abounahia, S. Mubashir, S. Fouladi, M. Khraisheh, Recent trends of copper detection in water samples, Bull. Natl. Res. Cent. 45 (1) (2021) 218, https://doi.org/10.1186/s42269-021-00677-w.

[15] L.A. Romero-Cano, A.I. Zárate-Guzmán, F. Carrasco-Marín, L.V. González-Gutiérrez, Electrochemical detection of copper in water using carbon paste electrodes prepared from bio-template (grapefruit peels) functionalized with carboxyl groups, J. Electroanal. Chem. 837 (2019) 22–29, https://doi.org/10.1016/j.jelechem.2019.02.005.

[16] R.T. Lima, J.L. Raposo Jr, A. Virgílio, J.A. Gomes Neto, Determination of copper at wide range concentrations using instrumental features of high-resolution continuum source flame atomic absorption spectrometry, Ecletica Quim. 35 (2010) 87–92, https://doi.org/10.1590/S0100-46702010000400011.

[17] C. Cui, M. He, B. Hu, Membrane solid phase microextraction with alumina hollow fiber online coupled with ICP-OES for the determination of trace copper, manganese and nickel in environmental water samples, J. Hazard Mater. 187 (1–3) (2011) 379–385, https://doi.org/10.1016/j.jhazmat.2011.01.038.

[18] J.E. O'Sullivan, R.J. Watson, E.C.V. Butler, An ICP-MS procedure to determine Cd, Co, Cu, Ni, Pb and Zn in oceanic waters using in-line flow-injection with solid-phase extraction for preconcentration, Talanta 115 (2013) 999–1010, https://doi.org/10.1016/j.talanta.2013.06.054.

[19] G.C. Midya, S. Paladhi, S. Bhowmik, S. Saha, J. Dash, Design and synthesis of an on–off "click" fluorophore that executes a logic operation and detects heavy and transition metal ions in water and living cells, Org. Biomol. Chem. 11 (18) (2013) 3057–3063, https://doi.org/10.1039/C3OB40075A.

[20] Y. Ma, H. Niu, Y. Cai, Colorimetric detection of copper ions in tap water during the synthesis of silver/dopamine nanoparticles, Chem. Commun. 47 (47) (2011) 12643–12645, https://doi.org/10.1039/C1CC15048K.

[21] P. Liu, R. Hao, W. Sun, J. Li, Ratiometric detection of Cu2+ in water and drinks using Tb (iii)-functionalized UiO-66-type meta-organic frameworks, Anal. Methods 15 (16) (2023) 1953–1958, https://doi.org/10.1039/D3AY00044C.

[22] Y. Sun, M. Wei, R. Liu, H. Wang, H. Li, Q. Kang, D. Shen, A smartphone-based ratiometric fluorescent device for field analysis of soluble copper in river water using carbon quantum dots as luminophore, Talanta 194 (2019) 452–460, https://doi.org/10.1016/j.talanta.2018.10.019.

[23] Z. Yao, B.S. Zhang, J.A. Prescher, Advances in bioluminescence imaging: new probes from old recipes, Curr. Opin. Chem. Biol. 45 (2018) 148–156, https://doi.org/10.1016/j.cbpa.2018.05.009.

[24] M.E. Frischer, J.M. Danforth, T.F. Foy, R. Juraske, Bioluminescent bacteria as indicators of chemical contamination of coastal waters, J. Environ. Qual. 34 (4) (2005) 1328–1336, https://doi.org/10.2134/jeq2004.0245.

[25] S. Prévéral, C. Brutesco, E.C.T. Descamps, C. Escoffier, D. Pignol, N. Ginet, D. Garcia, A bioluminescent arsenite biosensor designed for inline water analyzer, Environ. Sci. Pollut. Res. 24 (2017) 25–32, https://doi.org/10.1007/s11356-015-6000-7.

[26] R. Nishihara, R. Kurita, Mix-and-read bioluminescent copper detection platform using a caged coelenterazine analogue, Analyst 146 (20) (2021) 6139–6144, https://doi.org/10.1039/D1AN01292D.

[27] J.J. O'Sullivan, V. Medici, M.C. Heffern, A caged imidazopyrazinone for selective bioluminescence detection of labile extracellular copper (II), Chem. Sci. 13 (15) (2022) 4352–4363, https://doi.org/10.1039/D1SC07177G.

[28] J. Li, N. Wang, M. Xiong, M. Dai, C. Xie, Q. Wang, K. Quan, Y. Zhou, Z. Qing, A reaction-based ratiometric bioluminescent platform for point-of-care and quantitative detection using a smartphone, Anal. Chem. 95 (18) (2023) 7142–7149, https://doi.org/10.1021/acs.analchem.2c05422.

[29] Y. Ni, R. Arts, M. Merkx, Ratiometric bioluminescent sensor proteins based on intramolecular split luciferase complementation, ACS Sens. 4 (1) (2018) 20–25, https://doi.org/10.1021/acssensors.8b01381.

[30] M. Hattori, N. Sugiura, T. Wazawa, T. Matsuda, T. Nagai, Ratiometric bioluminescent indicator for a simple and rapid measurement of thrombin activity using a smartphone, Anal. Chem. 93 (40) (2021) 13520–13526, https://doi.org/10.1021/acs.analchem.1c02396.

[31] M.P. Hall, J. Unch, B.F. Binkowski, M.P. Valley, B.L. Butler, M.G. Wood, P. Otto, K. Zimmerman, G. Vidugiris, T. Machleidt, M.B. Robers, H.A. Benink, C.T. Eggers, M.R. Slater, P.L. Meisenheimer, D.H. Klaubert, F. Fan, L.P. Encell, K.V. Wood, Engineered luciferase reporter from a deep sea shrimp utilizing a novel imidazopyrazinone substrate, ACS Chem. Biol. 7 (2012) 1848–1857, https://doi.org/10.1021/cb3002478.

[32] K. Suzuki, T. Kimura, H. Shinoda, G. Bai, M.J. Daniels, Y. Arai, M. Nakano, T. Nagai, Five colour variants of bright luminescent protein for real-time multicolour bioimaging, Nat. Commun. 7 (1) (2016) 13718, https://doi.org/10.1038/ncomms13718.

[33] W. Ren, Z. Li, Y. Xu, D. Wan, B. Barnych, Y. Li, Z. Tu, Q. He, J. Fu, B.D. Hammock, One-step ultrasensitive bioluminescent enzyme immunoassay based on nanobody/nanoluciferase fusion for detection of aflatoxin B1 in cereal, J. Agric. Food Chem. 67 (18) (2019) 5221–5229, https://doi.org/10.1021/acs.jafc.9b00688.

[34] H. Sekhon, S.N. Loh, Engineering protein activity into off-the-shelf DNA devices, Cell Rep. Methods. 2 (4) (2022), https://doi.org/10.1016/j.crmeth.2022.100202.

[35] Y. Oh, Y. Park, J.H. Cho, H. Wu, N.K. Paulk, L.X. Liu, N. Kim, M.A. Kay, J.C. Wu, M. Z. Lin, An orange calcium-modulated bioluminescent indicator for non-invasive activity imaging, Nat. Chem. Biol. 15 (5) (2019) 433–436, https://doi.org/10.1038/s41589-019-0256-z.

[36] O. Shimomura, P.R. Flood, S. Inouye, B. Bryan, A. Shimomura, Isolation and properties of the luciferase stored in the ovary of the scyphozoan medusa Periphylla periphylla, Biol. Bull. 201 (3) (2001) 339–347, https://doi.org/10.2307/1543612.

[37] S. Inouye, S. Overexpression Sasaki, Purification and characterization of the catalytic component of Oplophorus luciferase in the deep-sea shrimp, Oplophorus gracilirostris, Protein Expr. Purif. 56 (2) (2007) 261–268, https://doi.org/10.1016/j.pep.2007.08.002.

[38] S. Inouye, Y. Sahara, Identification of two catalytic domains in a luciferase secreted by the copepod Gaussia princeps, Biochem. Biophys. Res. Commun. 365 (1) (2008) 96–101, https://doi.org/10.1016/j.bbrc.2007.10.152.

[39] A.A. Homaei, A.B. Mymandi, R. Sariri, E. Kamrani, R. Stevanato, S. Etezad, K. Khajeh, Purification and characterization of a novel thermostable luciferase from Benthosema pterotum, J. Photochem. Photobiol., B 125 (2013) 131–136, https://doi.org/10.1016/j.jphotobiol.2013.05.015.

[40] J.J. O'Sullivan, V.J. Lee, M.C. Heffern, Copper-mediated oxidation of imidazopyrazinones inhibits marine luciferase activity, Luminescence 38 (2) (2023) 216–220, https://doi.org/10.1002/bio.4415.
[41] Y. Ando, K. Niwa, N. Yamada, T. Irie, T. Enomoto, H. Kubota, Y. Ohmiya, H. Akiyama, Development of a quantitative bio/chemiluminescence spectrometer determining quantum yields: Re-examination of the aqueous luminol chemiluminescence standard, Photochem. Photobiol. 83 (5) (2007) 1205–1210, https://doi.org/10.1111/j.1751-1097.2007.00140.x.
[42] H. Zhao, T.C. Doyle, R.J. Wong, Y. Cao, D.K. Stevenson, D. Piwnica-Worms, C. H. Contag, Characterization of coelenterazine analogs for measurements of Renilla luciferase activity in live cells and living animals, Mol. Imag. 3 (1) (2004) 15353500200403181, https://doi.org/10.1162/15353500200403181.
[43] M. Nemergut, D. Pluskal, J. Horackova, T. Sustrova, J. Tulis, T. Barta, R. Baatallah, G. Gagnot, V. Novakova, M. Majerova, S.M. Marques, M. Toul, J. Damborsky, D. Bednar, Z. Prokop, Y.L. Janin, M. Marek, Illuminating the mechanism and allosteric behavior of NanoLuc luciferase, Nat. Commun. 14 (1) (2023) 7864, https://doi.org/10.1038/s41467-023-43403-y.
[44] A.S. Dixon, M.K. Schwinn, M.P. Hall, K. Zimmerman, P. Otto, T.H. Lubben, B. L. Butler, B.F. Binkowski, T. Machleidt, T.A. Kirkland, M.G. Wood, C.T. Eggers, L. P. Encell, K.V. Wood, NanoLuc complementation reporter optimized for accurate measurement of protein interactions in cells, ACS Chem. Biol. 11 (2) (2016) 400–408, https://doi.org/10.1021/acschembio.5b00753.
[45] N.C. Shaner, G.G. Lambert, A. Chammas, Y. Ni, P.J. Cranfill, M.A. Baird, B.R. Sell, J.R. Allen, R.N. Day, M. Israelsson, M.W. Davidson, J. Wang, A bright monomeric green fluorescent protein derived from Branchiostoma lanceolatum, Nat. Methods 10 (5) (2013) 407–409, https://doi.org/10.1038/nmeth.2413.
[46] I. Hamidah, A. Solehudin, A. Hamdani, L. Hasanah, K. Khairurrijal, T. Kurniawan, R. Mamat, R. Maryanti, A.B.D. Nandiyanto, B. Hammouti, Corrosion of copper alloys in KOH, NaOH, NaCl, and HCl electrolyte solutions and its impact to the mechanical properties, Alex. Eng. J. 60 (2) (2021) 2235–2243, https://doi.org/10.1016/j.aej.2020.12.027.